

# Upper limits on dark energy-dark matter interaction from DESI DR2 in a field-theoretic analysis

Amin Aboubrahim<sup>a\*</sup> and Pran Nath<sup>b†</sup>

<sup>a</sup>*Department of Physics and Astronomy, Union College,  
807 Union Street, Schenectady, NY 12308, U.S.A.*

<sup>b</sup>*Department of Physics, Northeastern University,  
111 Forsyth Street, Boston, MA 02115-5000, U.S.A.*

## Abstract

One of the important issues both in particle physics and cosmology relates to whether dark energy is a cosmological constant  $\Lambda$ , or is dynamical in nature such as quintessence. In this work, we discuss a model of quintessence interacting with dark matter and analyze the resulting phenomenology of the dark energy equation of state. We identify two regions where the equation of state behaves differently depending on the size of the dark matter-dark energy interaction strength. We show that the strong coupling region induces a transmutation of quintessence from thawing to freezing. Using the recent data release from the Dark Energy Spectroscopic Instrument (DESI), we rule out this possibility of transmutation and investigate the weak coupling region to derive upper limits on the interaction strength. The interacting dark energy model is able to explain DESI's results without the equation of state crossing the phantom divide.

---

\*[abouibra@union.edu](mailto:abouibra@union.edu)

†[p.nath@northeastern.edu](mailto:p.nath@northeastern.edu)

---

# Contents

<b>1</b>	<b>Introduction</b>	<b>2</b>
<b>2</b>	<b>The model</b>	<b>4</b>
<b>3</b>	<b>Field-theoretic inconsistency of the fluid model</b>	<b>5</b>
<b>4</b>	<b>Dark matter and dark energy background equations</b>	<b>5</b>
<b>5</b>	<b>Cosmological evolution of interacting dark energy and dark matter</b>	<b>7</b>
5.1	The strong coupling regime . . . . .	7
5.2	The weak coupling regime . . . . .	12
<b>6</b>	<b>Conclusion</b>	<b>17</b>
<b>A</b>	<b>Background equations for a general dark matter potential</b>	<b>18</b>
<b>B</b>	<b>Comparison between QCDM and the phenomenological model</b>	<b>20</b>
<b>C</b>	<b>Correlation plots</b>	<b>21</b>

---

## 1 Introduction

Currently the concordance  $\Lambda$ CDM model is considered the Standard Model of cosmology and is successful at explaining a large amount of cosmological data. It is described by the action

$$S_{\Lambda\text{CDM}} = \int d^4x \sqrt{-g} \left[ \frac{1}{16\pi G} (R - 2\Lambda) + \mathcal{L}_{\text{CDM}} \right], \quad (1.1)$$

where  $g = \det(g^{\mu\nu})$  is the determinant of the metric  $g^{\mu\nu}$ . We use the Friedmann-Lemaître-Robertson-Walker metric in conformal time  $\tau$  so that the line element is given by  $ds^2 = a^2(\tau) [-d\tau^2 + g_{ij}dx^i dx^j]$ , where  $a(\tau)$  is the scale factor. In Eq. (1.1),  $R$  is the Ricci scalar,  $G$  is Newton’s constant,  $\Lambda$  is the Einstein cosmological constant, and  $\mathcal{L}_{\text{CDM}}$  is the Lagrangian density for Cold Dark Matter (CDM). More generally,  $\mathcal{L}_{\text{CDM}}$  can be replaced by the Lagrangian density  $\mathcal{L}_m$  which includes all forms of matter and radiation. In spite of the great success of Eq. (1.1), some anomalies have recently emerged, with two of the prominent ones being the Hubble tension,  $H_0$ , and the degree of matter clustering,  $S_8$  [1, 2]. Several suggestions to reduce the Hubble tension have been proposed which, to name a few, include interacting dark matter models [3–29], early dark energy [30–32], decaying dark matter [33, 34] as well as models introducing extra relativistic degrees of freedom [35–43]. A current trend is to introduce an interaction term (or a source term) between dark matter (DM) and dark

energy (DE) at the level of the continuity equations [1, 16, 44, 45], so that

$$\rho'_\chi + 3\mathcal{H}(1 + w_\chi)\rho_\chi = Q, \quad (1.2)$$

$$\rho'_\phi + 3\mathcal{H}(1 + w_\phi)\rho_\phi = -Q. \quad (1.3)$$

Here  $\rho_\chi$  and  $\rho_\phi$  are the energy densities for DM and DE,  $w_\chi$  and  $w_\phi$  are the corresponding equations of state (EoS), with  $w$  defined as the ratio of pressure ( $p$ ) to energy density ( $\rho$ ) for a given species,  $w = p/\rho$ , and  $' \equiv d/d\tau$ . However, in Eqs. (1.2) and (1.3), the energy conservation is imposed in an ad hoc manner by choosing the sources to be  $+Q$  and  $-Q$  and these equations are inconsistent within a field theoretic framework.

Other than the  $H_0$  and  $S_8$  tensions, other anomalies have emerged as well, specifically one related to the dark energy EoS. Thus, the Dark Energy Spectroscopic Instrument (DESI) [46, 47] recent results have pointed toward a time-varying EoS. In  $\Lambda$ CDM, the cosmological constant's EoS is  $w_\Lambda = -1$  and so a time-varying  $w$  may indicate some underlying new physics deviating from  $\Lambda$ CDM. Using the Chevallier-Polarski-Linder (CPL) parameterization [48, 49] of the EoS,  $w(a) = w_0 + (1 - a)w_a$ , DESI DR1 reports a preference for  $w_0 > -1$  and  $w_a < 0$  with the DESI BAO + CMB + DESY5 data set at the  $3.9\sigma$  level which grew to  $4.2\sigma$  with DR2. Quintessence is a well known alternative to the cosmological constant which can provide a scenario for a dynamical EoS. Many models have been proposed in this direction leading to several classifications of quintessence models. Thus in thawing quintessence [50–53], the field is initially frozen due to the Hubble friction so that  $w_\phi \simeq -1$ . The mass of the field then becomes smaller than  $\mathcal{H}$  at late times causing a deviation of  $w_\phi$  away from  $-1$ . In freezing models,  $w_\phi$  decreases towards  $-1$  at late times because of the shallow nature of the potential which, for a scaling freezing model [54, 55], is taken to be a double exponential potential. Compared to CPL, these models produce more complicated parameterizations of the EoS which do not lead to the crossing of the phantom divide, something the CPL suffers from.

In this work, we examine the impact of a field-theoretic model on cosmology, and in particular, we focus on the dark energy equation of state. Motivated by a previous work [56, 57], where the authors have shown that such a field-theoretic approach can alleviate the  $H_0$  tension and resolve the  $S_8$  tension, we set out to explore the possibility of a dynamical EoS. Furthermore, we drop Eqs. (1.2) and (1.3) which are inconsistent within a field theoretic framework and consider a field theoretic formulation where energy conservation is automatic. We show that in this framework DM-DE interaction can lead to a rich EoS phenomenology, where for a strong coupling, a transmutation of quintessence from thawing to scaling freezing occurs while a weaker coupling retains the thawing nature of quintessence. We investigate fits to the EoS in the two coupling regimes and examine the impact of the DM-DE coupling in bringing the model to agreement with DESI DR2. We show that while the DM-DE interaction can be an impactful parameter in aligning model predictions with DESI's results, a strong preference exists for non-interacting quintessence to explain DESI's DR2 results.

## 2 The model

In the analysis here we propose an alternative to  $\Lambda$ CDM of Eq. (1.1) which is a model of quintessence interacting with dark matter (QCDM) based on a Lagrangian. Thus we consider a set of  $n$  interacting spin zero fields  $\phi_i$  ( $i = 1 \cdots n$ ) where one of the fields is the quintessence field and the rest are matter fields which may contain one or more dark matter fields and the rest may be other forms of matter fields. The action of this theory is given by

$$S_{\text{QCDM}} = \int d^4x \sqrt{-g} \left[ \frac{1}{16\pi G} R + \mathcal{L}_{\text{QCDM}} \right], \quad (2.1)$$

and the QCDM Lagrangian is

$$\mathcal{L}_{\text{QCDM}} = \sum_i \frac{1}{2} \phi_i^\mu \phi_{i,\mu} - V(\{\phi_i\}, \{\phi_j\}), \quad (2.2)$$

where

$$V = \sum_i^n V_i(\phi_i) + V_{\text{int}}(\{\phi_i\}, \{\phi_j\}), \quad (2.3)$$

$$V_{\text{int}}(\{\phi_i\}, \{\phi_j\}) = \frac{1}{2} \sum_{i \neq j} \sum_j V_{ij}(\phi_i, \phi_j), \quad (2.4)$$

with  $V_{ij}(\phi_i, \phi_j)$  being the interaction potential between the fields  $\phi_i$  and  $\phi_j$ . The Klein-Gordon equation for the field  $\phi_i$  is given by

$$\phi_i'' + 2\mathcal{H}\phi_i' + a^2 \left( V_{i,\phi_i} + \frac{1}{2} \sum_{j \neq i} (V_{ij} + V_{ji}, \phi_i) \right) = 0, \quad (2.5)$$

where  $V_{ij,\phi_i} \equiv \partial_{\phi_i} V_{ij}$ , and  $\mathcal{H} = a'/a$  is the conformal Hubble parameter. Assuming  $V_{ji} = V_{ij}$ , the corresponding continuity equations are then given by

$$\rho_i' + 3\mathcal{H}(1 + w_i)\rho_i = Q_i, \quad (2.6)$$

$$Q_i = \sum_{j \neq i} V_{ij,\phi_j}(\phi_i, \phi_j) \phi_j'. \quad (2.7)$$

Here the energy density  $\rho_i$  and the pressure  $p_i$  for the energy density of field  $\phi_i$  are given by

$$\rho_i(p_i) = T_i \pm V_i(\phi_i) \pm \sum_{j \neq i} V_{ij}(\phi_i, \phi_j), \quad (2.8)$$

where  $T_i$  is the kinetic energy of field  $\phi_i$ , the  $+(-)$  signs are for the cases  $\rho_i$  ( $p_i$ ), and  $w_i = p_i/\rho_i$ . The total energy density is then defined by

$$\rho = \sum_i \rho_i - \sum_{i < j} V_{ij}(\phi_i, \phi_j), \quad (2.9)$$

where the last term on the right hand side is included to ensure no double counting. Eq. (2.9) is a generalization of the two-field case [56] to the case of  $n$ -interacting fields. The observed relic density for the particle  $i$  is given by

$$\Omega_{0i} = \frac{\rho_i}{\rho_{0,\text{crit}}}(1 - \delta_i), \quad \sum_i \Omega_{0i} = 1, \quad \delta_i = \frac{\sum_{j \neq i} V_{ij}}{\sum_j \rho_j}. \quad (2.10)$$

Eqs. (2.6) and (2.7) are a consistent set of continuity equations for the case of  $n$  number of interacting fields, where the energy density  $\rho_i$  corresponds to the field  $\phi_i$ .

### 3 Field-theoretic inconsistency of the fluid model

In order to include interactions, the phenomenological fluid model uses the continuity equations of the  $\Lambda$ CDM model but includes interactions by assuming a set of ad hoc sources for them. To achieve conservation of energy, one then assumes that  $\rho = \sum_i \rho_i$  and imposes the condition that the sum of the sources vanishes, i.e.,  $\sum_i Q_i = 0$  which implies using Eq. (2.6) without knowledge of Eq. (2.7). In field theory,  $\sum_i Q_i = 0$  leads to

$$V'_{\text{int}}(\{\phi_i\}, \{\phi_j\}) = 0, \quad (3.1)$$

which means that  $V_{\text{int}}$  is a constant (independent of time). This is obviously incorrect since it depends on  $n$  number of fields each of which is time-dependent and there is no reason why  $V_{\text{int}}(\phi_i, \phi_j)$  would be independent of time. We illustrate this with an example of two interacting fields  $\chi$  and  $\phi$  with an interacting potential

$$V_{\text{int}}(\phi, \chi) = \frac{\lambda}{2} \chi^2 \phi^2, \quad (3.2)$$

one of which ( $\chi$ ) will act as dark matter and the other ( $\phi$ ) as dark energy or quintessence [51, 58, 59]. In this case  $Q_\chi$  and  $Q_\phi$  are given by

$$Q_\chi = V_{\text{int},\phi} \phi'_0, \quad Q_\phi = V_{\text{int},\chi} \chi'_0. \quad (3.3)$$

From Eq. (3.1), we have  $V'_{\text{int}}(\chi, \phi) = 0$ , i.e.,  $V_{\text{int}}(\chi, \phi)$  is independent of time and so we write

$$V_{\text{int}}(\chi, \phi) = \frac{\lambda}{2} \chi^2 \phi^2 = c. \quad (3.4)$$

Here  $c$  is a constant which gives  $\chi = \pm \sqrt{\frac{2c}{\lambda}} \phi$ , i.e., the fields  $\chi$  and  $\phi$  are not independent but one is determined in terms of the other which is obviously false. Thus the fluid equations, Eq. (1.2) and Eq. (1.3), are inconsistent within a field theoretic framework.

### 4 Dark matter and dark energy background equations

In this section, we derive the background equations that describe the time evolution of the DM and DE fields in a flat FLRW metric. In our interacting quintessence-dark matter model

(QCDM),  $\chi$  represents a dark matter field while  $\phi$  is a dark energy field and are governed by the potentials

$$V_1(\chi) = \frac{1}{2}m_\chi^2\chi^2, \quad (4.1)$$

$$V_2(\phi) = \mu^4 \left[ 1 + \cos\left(\frac{\phi}{F}\right) \right]. \quad (4.2)$$

The interaction potential between  $\chi$  and  $\phi$  is based on field theory and is given by

$$V_{\text{int}}(\phi, \chi) \equiv V_{12}(\phi, \chi) = \frac{\lambda}{2}\chi^2\phi^2. \quad (4.3)$$

We track the evolution of the two background fields  $\chi$  and  $\phi$  by solving the Klein-Gordon (KG) equations

$$\chi_0'' + 2\mathcal{H}\chi_0' + a^2(V_{1,\chi} + V_{12,\chi}) = 0, \quad (4.4)$$

$$\phi_0'' + 2\mathcal{H}\phi_0' + a^2(V_{2,\phi} + V_{12,\phi}) = 0, \quad (4.5)$$

where the ‘0’ subscript denotes a background field. For a DM potential of the form given by Eq. (4.1), the field undergoes rapid oscillations when  $\mathcal{H}/m_\chi \ll 1$  [60,61], making a numerical solution intractable. In order to efficiently solve the background evolution equation for the DM field, we recast Eq. (4.4) in a different form. First, let us define the DM energy density as  $\tilde{\rho}_\chi = \rho_\chi - V_{12}$  so that the modified energy density fraction becomes

$$\tilde{\Omega}_\chi \equiv \frac{\tilde{\rho}_\chi}{\rho_{\text{cr}}} = \frac{\kappa^2}{6\mathcal{H}^2} \left( \chi_0'^2 + 2a^2V_1(\chi_0) \right), \quad (4.6)$$

where  $\kappa \equiv \sqrt{8\pi G}$ . Based on Eq. (4.6), we define the following new dimensionless variables [24,55]

$$\tilde{\Omega}_\chi^{1/2} \sin\left(\frac{\theta}{2}\right) = \frac{\kappa\chi'}{\sqrt{6}\mathcal{H}}, \quad (4.7)$$

$$\tilde{\Omega}_\chi^{1/2} \cos\left(\frac{\theta}{2}\right) = \frac{\kappa a V_1^{1/2}}{\sqrt{3}\mathcal{H}}, \quad (4.8)$$

$$y = -\frac{2\sqrt{2}a}{\mathcal{H}}\partial_\chi V_1^{1/2}. \quad (4.9)$$

The advantage gained by introducing the new variables is that the rapid oscillations of the DM field can be absorbed into the  $\theta$  variable. Using the new variables defined by Eqs. (4.7)–(4.9), we recast the KG equation of the field  $\chi$  into a set of three coupled first order differential equations in  $\Omega_\chi$ ,  $\theta$  and  $y$ . After some lengthy, but otherwise straightforward, calculation, we arrive at

$$\Omega_\chi' = 3\mathcal{H}\Omega_\chi(w_T - w_\chi) + \frac{\kappa^2 a^2}{3\mathcal{H}^2} \left[ \mathcal{H}(1 + 3w_\chi)V_{12} - \chi'V_{12,\chi} \right], \quad (4.10)$$

$$\theta' = -3\mathcal{H}\sin\theta + \mathcal{H}y - \frac{\kappa^2 a^2}{3\mathcal{H}^2\tilde{\Omega}_\chi} \left( 2\mathcal{H}V_{12} + \chi'V_{12,\chi} \right) \cot\frac{\theta}{2}, \quad (4.11)$$

$$y' = \frac{3}{2}\mathcal{H}(1 + w_T)y, \quad (4.12)$$

with the total EoS  $w_T = \sum p_i / \sum \rho_i$ , where the sum is over all species (baryons, photons, neutrinos, DM and DE) and  $\tilde{\Omega}_\chi = \Omega_\chi - (\kappa^2 a^2 / 3\mathcal{H}^2) V_{12}$ . Note that the last set of terms in each of Eqs. (4.10) and (4.11) represent the interaction term. In terms of the new variables, the DM equation of state  $w_\chi$  can be written as

$$w_\chi = \frac{\tilde{p}_\chi}{\tilde{\rho}_\chi} = \frac{\frac{1}{2a^2}\chi'^2 - V_1(\chi)}{\frac{1}{2a^2}\chi'^2 + V_1(\chi)} = -\cos\theta. \quad (4.13)$$

With the rapid oscillations absorbed into the  $\theta$  parameter, the DM equation of state oscillates between +1 and -1, so that the time-average of  $w_\chi$  becomes zero, thus describing a pressureless fluid, i.e., CDM.

## 5 Cosmological evolution of interacting dark energy and dark matter

We are now in a position to solve Eqs. (4.10), (4.11) and (4.12) to track the evolution of the DM field  $\chi$ , and the KG equation, Eq. (4.5), to determine the evolution of the DE field. We implement and solve the above equations in the Boltzmann equation solver CLASS [62] in order to determine the evolution of the DM and DE fields as well as the SM species (photons, baryons and neutrinos). To make sure the closure relation  $\sum_i \Omega_i = 1$  is satisfied, we use the shooting method in CLASS to evolve the background equations starting from  $a_{\text{ini}} = 10^{-14}$  to  $a_0 = 1$  (today). The shooting variable is  $\Omega_\chi$  and a quantity  $\mathcal{O}(10^{-2})$  is varied during the shooting process in order to achieve today's DM abundance  $\Omega_{\chi 0} \sim 0.26$ . We use the attractor initial conditions [61] for the field  $\chi$  with

$$y_{\text{ini}} = \frac{2m_\chi}{H_0} a_{\text{ini}}^2 \Omega_{\text{rad}0}^{-1/2}, \quad (5.1)$$

$$\theta_{\text{ini}} = \frac{1}{5} y_{\text{ini}}, \quad (5.2)$$

$$\Omega_{\chi\text{ini}} = a_{\text{ini}} \frac{\Omega_{\chi 0}}{\Omega_{\text{rad}0}} \left[ \frac{4\theta_{\text{ini}}^2}{\pi^2} \left( \frac{9 + \pi^2/4}{9 + \theta_{\text{ini}}^2} \right) \right]^{3/4}, \quad (5.3)$$

where the index '0' indicates a quantity's value today and 'rad' stands for radiation. For the DE field  $\phi$ , we choose the initial conditions  $\phi_{\text{ini}}$  and  $\phi'_{\text{ini}} = 10^{-3}$  and an estimate of  $\mu^4$  is determined by minimizing the DE potential so that  $\mu^4 = \frac{3}{2} H_0^2 \Omega_{\phi 0}$ . This value serves as an initial estimate and we modify  $\mu^4$  accordingly in order to achieve a consistent cosmology.

### 5.1 The strong coupling regime

The DM-DE coupling strength,  $\lambda$ , enters Eqs. (4.5), (4.10) and (4.11) through the term  $V_{12}$  and affects the DE EoS through

$$w_\phi \equiv \frac{p_\phi}{\rho_\phi} = \frac{\frac{1}{2a^2}\phi'^2 + V_2 + V_{12}}{\frac{1}{2a^2}\phi'^2 - V_2 - V_{12}}. \quad (5.4)$$

Before going in depth into analyzing the effect of  $\lambda$  on  $w_\phi$ , we discuss some of the important observables and their evolution for three values of  $\phi_{\text{ini}}$  and  $\mu^4$  (expressed in standard CLASS units of  $m_{\text{pl}}$  and  $m_{\text{pl}}^2/\text{Mpc}^2$ , respectively) with non-zero DM-DE interaction, i.e.,  $\lambda > 0$ . Here we choose  $\lambda > 10^{-2}$  which corresponds to the strong coupling regime.

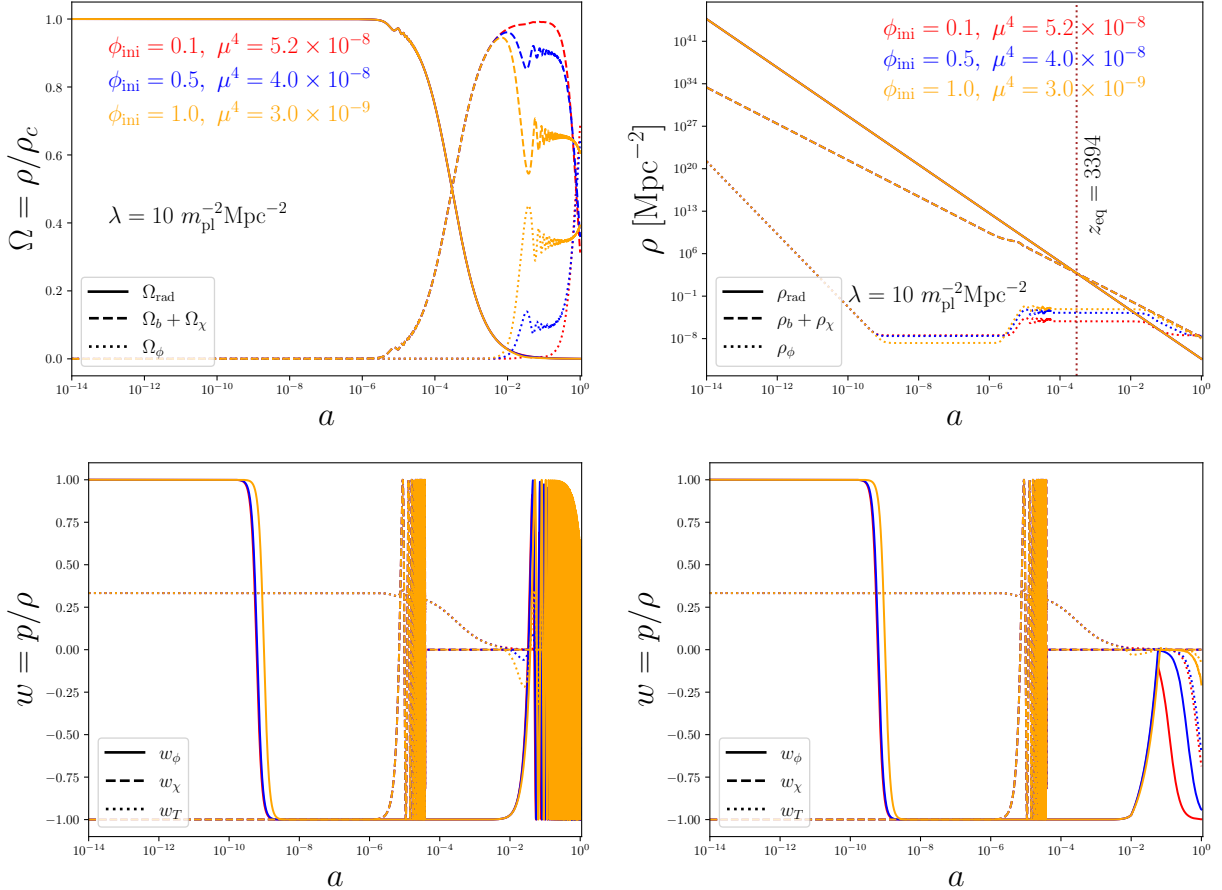


**Figure 1:** Top panels: plot of the energy density fractions (left) and the energy densities evolution (right) as a function of the scale factor  $a$ . Bottom panels: plot of the evolution of the equations of state (EoS) of DM and DE and the total EoS (left) and a time-average over the oscillations in  $w_\phi$  and  $w_T$  (right panel). The color code in the top panel is the same for the bottom panel and correspond to different values of  $\phi_{\text{ini}}$  and  $\mu^4$  in the presence of DM-DE interaction, expressed in standard CLASS units of  $m_{\text{pl}}$  and  $m_{\text{pl}}^2/\text{Mpc}^2$ , respectively.

In the top panel of Fig. 1, we exhibit the evolution of the energy density fraction (left) and of the energy density (right) for baryons, photons, DM and DE. Similar to  $\Lambda$ CDM, the QCDM model predicts the redshift of matter-radiation equality to be  $z_{\text{eq}} \sim 3390$  consistent with Planck's measurements. Larger values of  $\phi_{\text{ini}}$  lead to larger  $\Omega_{\phi 0}$  and thus smaller  $\Omega_{\chi 0}$  so that the closure relation holds. The oscillatory feature in  $\Omega$  can be explained by examining the bottom left panel which shows the equation of state (EoS) of DM, DE and the total EoS. At early times,  $w_\chi = -1$  and  $w_\phi = +1$  and so the  $\phi$  field acts as radiation while the  $\chi$  field acts as an early DE component for a period of time before the onset of rapid oscillations

at around  $a \sim 10^{-5}$ . Averaging the fast oscillations in  $\chi$  renders  $w_\chi = 0$  and so the  $\chi$  field eventually dilutes as CDM, i.e.,  $\rho_\chi \sim a^{-3}$ . The imprints of these rapid oscillations are visible as little wiggles in the energy density plots in the left-hand-side of the top panel. The  $\phi$  field, on the other hand, starts off as radiation and as the DE potential rolls down to its minimum, the EoS drops to  $-1$ . The interesting feature here is that similar to  $\chi$ , the DE field begins to oscillate but at a later time, around  $a \sim 10^{-2}$ . The difference between the oscillations of the  $\chi$  and  $\phi$  fields is that while the amplitude of oscillations of  $w_\chi$  is constant, that of  $\phi$  is decaying. Averaging over these oscillations, we display in Fig. 1 (bottom right panel) the variations in  $w_\phi$  where one can see  $w_\phi$  departing away from  $-1$  before turning around and decreasing again toward  $-1$ . One finds that for  $\phi_{\text{ini}} = 0.1$ ,  $w_\phi$  decays to  $-1$  as one would expect from a DE component, while for  $\phi_{\text{ini}} = 0.5$  we get  $w_\phi \sim -0.9$ . However, for  $\phi_{\text{ini}} = 1.0$ , the oscillations remain strong even at  $a = 1$  and even though the averaged  $w_\phi$  is less than zero, it is still much larger than  $-1$ , which is the well accepted value from observations. Therefore, one can easily reject  $\phi_{\text{ini}} = 1.0$  and only consider smaller  $\phi_{\text{ini}}$ . Note that even when the oscillations in  $\Omega_\chi$  have been averaged out, they reappear once  $\Omega_\phi$  starts its oscillations because the fields are coupled.

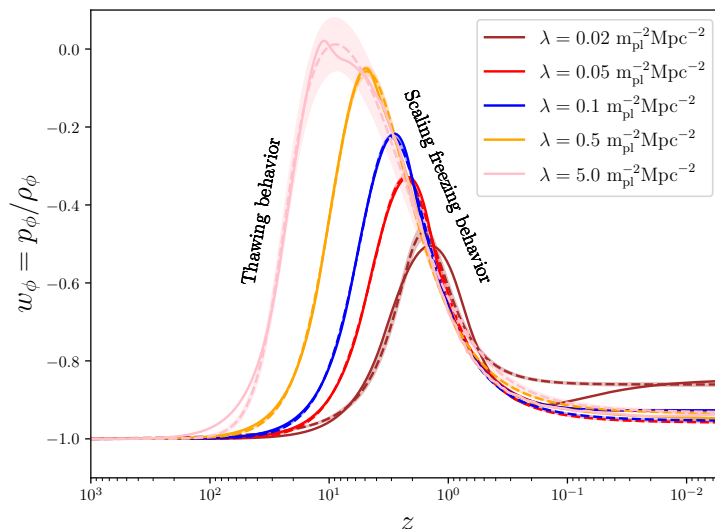


**Figure 2:** Evolution of  $w_\phi$  for quintessence for five values of  $\lambda$  as a function of the redshift  $z$ . The solid lines are  $w_\phi$  predicted by QCDM and the dashed lines are fits based on Eq. (5.5) including a  $1\sigma$  error band around each curve. In each case, quintessence transmutes from thawing (left shoulder) to scaling freezing (right shoulder) induced by  $\lambda$ .

We now address the peculiar evolution of  $w_\phi$  seen in the lower right panel of Fig. 1 for  $a > 10^{-2}$ . We show in Fig. 2 the evolution of the DE equation of state as a function of the redshift  $z = 1/a - 1$  for five values of the interaction strength  $\lambda$  (solid curves) with the dashed curves representing the fits to the data from the QCDM model. The fit is given by

$$w(a) = -1 + \frac{\alpha a^p e^{-pa}}{1 + (\beta a)^q}, \quad (5.5)$$

where  $\alpha$ ,  $\beta$ ,  $p$  and  $q$  are the fit parameters. It is clear that for the considered benchmarks, the EoS departs away from  $w_\phi = -1$  in the range  $10 < z < 100$  tracking a thawing quintessence behavior, before turning around and falling back toward  $w_\phi \sim -1$  at late times, a behavior similar to scaling freezing. The presence of a DM-DE interaction term has induced a transmutation of the DE from thawing to scaling freezing. A quintessence with a scaling freezing behavior at current times is not favored by the recent DESI data.

To see this, we examine two cases: when no DM-DE interaction is presented and when the interaction is switched on. The first scenario is shown in the left panel of Fig. 3 and the second in the right panel of Fig. 3, where we exhibit the evolution of the DE EoS between  $a = 0.1$  and  $a = 1$ . The green band shows the  $1\sigma$  range of the allowed values of  $w_\phi$  as obtained from the combination of the data set DESI + CMB + PantheonPlus under the  $w$ CDM assumption ( $w_\phi = \text{constant}$ ), which is consistent with the baseline  $\Lambda$ CDM. The blue band corresponds to DESI's  $1\sigma$  values of  $w_0$  and  $w_a$  in the CPL parametrization, given by  $w(a) = w_0 + (1 - a)w_a$  (dubbed  $w_0w_a$ CDM).

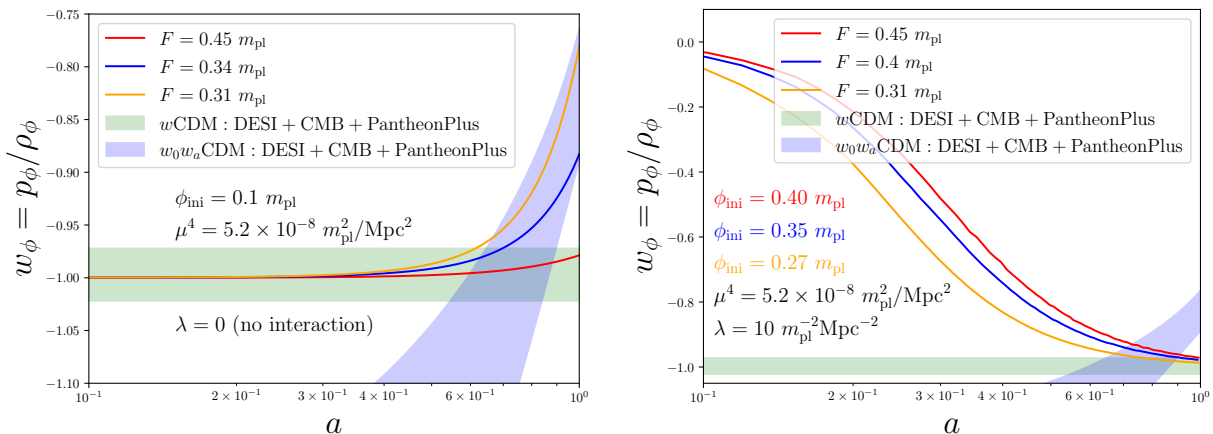


**Figure 3:** A plot of the EoS of  $\phi$  as a function of the scale factor  $a$  exhibiting the thawing behavior (left) when  $\lambda = 0$  and scaling freezing (right) when  $\lambda \neq 0$ . The  $1\sigma$  regions from DESI are shown as blue and green bands. A comparison of the left and the right panels indicates that the EoS of dark energy is sensitively dependent on the DE-DM interaction strength.

In the absence of DM-DE interaction (left panel), the EoS tracks  $w_\phi = -1$  before it starts to deviate away from it close to  $a = 0.3$  which is consistent with thawing models with a pseudo-Nambu-Goldstone boson potential [63]. The benchmark in red is consistent with the DESI  $w$ CDM result<sup>1</sup> (green band), while the other two benchmarks show major deviation away from  $w_\phi = -1$  and are consistent with  $w_0w_a$ CDM near  $a = 1$ . When the DM-DE interaction is switched on (right panel), we notice that the dynamics of the EoS changes significantly. The evolution of  $w_\phi$  becomes consistent with scaling freezing models [55, 69], where the EoS slowly approaches  $w_\phi = -1$  as  $a \rightarrow 1$ . Therefore, the presence of the interaction term has modified the DE potential in such a way that the new behavior now

<sup>1</sup>Fits to DESI results have been carried out recently for quintessence, e.g. in refs. [64–68].

resembles that of scaling freezing models with an evolution that fits well a double exponential potential  $V_S(\phi) = \tilde{V}_0(e^{-\lambda_1\phi} + e^{-\lambda_2\phi})$ . Note that both the thawing and scaling freezing modes pertaining to  $w_\phi$  appear in the lower right panel of Fig. 1 where there is a clear transition from thawing to scaling freezing near  $a_t \sim 0.1$  for non-zero interaction. Analytically, one can see this behavior by expanding the potentials around the minimum, so that

$$V_2(\phi) + V_{12}(\phi, \chi) = \mu^4 \left[ 1 + \cos\left(\frac{\phi}{F}\right) \right] + \frac{\lambda}{2}\chi^2\phi^2 \simeq 2\mu^4 + V_0\phi^2, \quad (5.6)$$

where  $V_0 = (\lambda\chi^2/2 - \mu^4/2F^2)$ . Fitting the  $\Lambda$ CDM model data to the double exponential potential, we find that  $\lambda_1 = -\lambda_2$ , and so

$$V_S(\phi) = \tilde{V}_0(e^{-\lambda_1\phi} + e^{\lambda_1\phi}) = 2\tilde{V}_0 \cosh(\lambda_1\phi) \simeq 2\tilde{V}_0 + \tilde{V}_0\lambda_1^2\phi^2. \quad (5.7)$$

Notice that Eqs. (5.6) and (5.7) describe the same physics which explains the transition between thawing and scaling freezing quintessence in the late universe.

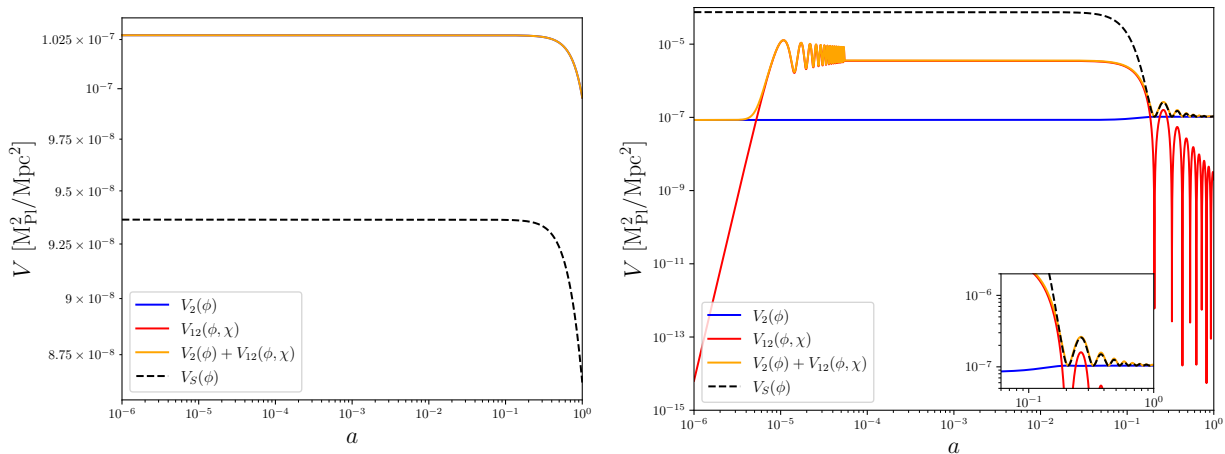


**Figure 4:** Left panel versus right panel correspond to the no interaction versus non-zero interaction cases. The evolution of the quintessence potential  $V_2(\phi)$  (blue), the interaction potential  $V_{12} = \lambda\phi^2\chi^2/2$  (red) and the total potential (orange) as a function of the scale factor  $a$ . The potential  $V_S(\phi) = \tilde{V}_0(e^{-\lambda_1\phi} + e^{-\lambda_2\phi})$  (black dashed) is fitted to the total potential, where  $\lambda_1 = -\lambda_2 = -18.2 \text{ m}_{\text{pl}}^{-1}$ . The fit works very well for  $a > 0.1$  (inset of right panel).

In Fig. 4, we show a plot for the potential versus  $a$  when no DM-DE interaction is present (left panel) and when the interaction is switch on (right panel). The total potential shown as an orange curve in the right panel has a decaying oscillatory feature close to  $a = 1$  and a double exponential function,  $V_S(\phi)$ , shown as a black dashed curve, exactly fits the total potential in that region, which can also be clearly seen in the figure inset. There,  $V_2 + V_{12} \sim \phi^2$  which is exactly the behavior of the scaling freezing double exponential potential for  $\lambda_1 = -\lambda_2$ .

Based on DESI DR1 and DR2, a DE quintessence with a freezing behavior is inconsistent with the existing constraints on  $w_0$  and  $w_a$ . Our model, however, has several free parameters,

namely:  $F$ ,  $\phi_{\text{ini}}$ ,  $\mu^4$  and  $\lambda$ . We thoroughly checked that no parameter combination can be chosen that will fit the  $w_0$  and  $w_a$  values in the strong coupling regime. We did so by expanding Eq. (5.5) around  $\epsilon = (1 - a)$  up to linear order. We get

$$w_0 = -1 + \frac{\alpha e^{-p}}{1 + \beta^q}, \quad (5.8)$$

$$w_a = \frac{q\beta^q}{1 + \beta^q}(1 + w_0). \quad (5.9)$$

From the above we see that the current DESI analysis fixes two of the four parameters of Eq. (5.5). Thus, for example, one may use  $w_0$  and  $w_a$  to determine  $\beta^q$  using Eq. (5.9) and use Eq. (5.8) to determine  $e^{-p}$ . This leaves us with two unconstrained parameters  $\alpha$  and  $q$ . Knowing the values of  $w_0$  and  $w_a$  from DESI, we tried to fit our model data using  $\alpha$  and  $q$  and found that one cannot get any good fit in the strong coupling regime. As expected, the current DESI data does not favor quintessence with a scaling freezing behavior.

## 5.2 The weak coupling regime

We have seen in the previous section that a strong DM-DE coupling turns a thawing quintessence into freezing at late time which is problematic from an observational perspective. In the absence of a DM-DE interaction, quintessence with potential of the form given by Eq. (4.2) give rise to a thawing behavior as depicted in the left panel of Fig. 3. In this section we will answer the following questions: (1) How large can the DM-DE interaction strength,  $\lambda$ , be while still remaining consistent with DESI's data within  $2\sigma$ , and (2) does any of the data sets in DESI's analysis prefer a non-zero  $\lambda$ ? We approach the latter question by investigating the impact of  $\lambda$  and the other three input parameters:  $F$ ,  $\phi_{\text{ini}}$  and  $\mu^4$  in driving the  $w_0$  and  $w_a$  values to fall within DESI's  $2\sigma$  bounds.

We run a MCMC analysis of the model parameter space while restricting the sampling to the weak coupling regime, i.e.,  $\lambda \leq 10^{-2}$ . We find that in this regime, the dark energy EoS can be fitted by the function

$$\hat{w}(a) = -1 + \alpha e^{-\beta a} \arctan(p a^q), \quad (5.10)$$

with  $\alpha$ ,  $\beta$ ,  $p$  and  $q$  being the fit parameters. Expanding Eq. (5.10) up to first order in  $(1 - a)$ , we get  $w_0$  and  $w_a$  so that

$$w_0 = -1 + \alpha e^{-\beta} \arctan(p), \quad (5.11)$$

$$w_a = \frac{\alpha e^{-\beta}}{1 + p^2} \left[ -p q + \beta(1 + p^2) \arctan(p) \right]. \quad (5.12)$$

We fit the DE EoS,  $w_\phi(a)$ , obtained from our model to the equation  $\hat{w}(a) = w_0 + (1 - a)w_a$  and determine the values of  $w_0$  and  $w_a$  of each model data point. The data point whose fit minimizes the  $\chi^2$  value

$$\chi^2 = \sum_i \left( \frac{w_i(a) - \hat{w}_i(a)}{\sigma_i} \right)^2 \quad (5.13)$$

is retained. We give in Fig. 5 a scatter plot in the  $w_0$ - $w_a$  plane of the model data points which are a good fit to the DE EoS.

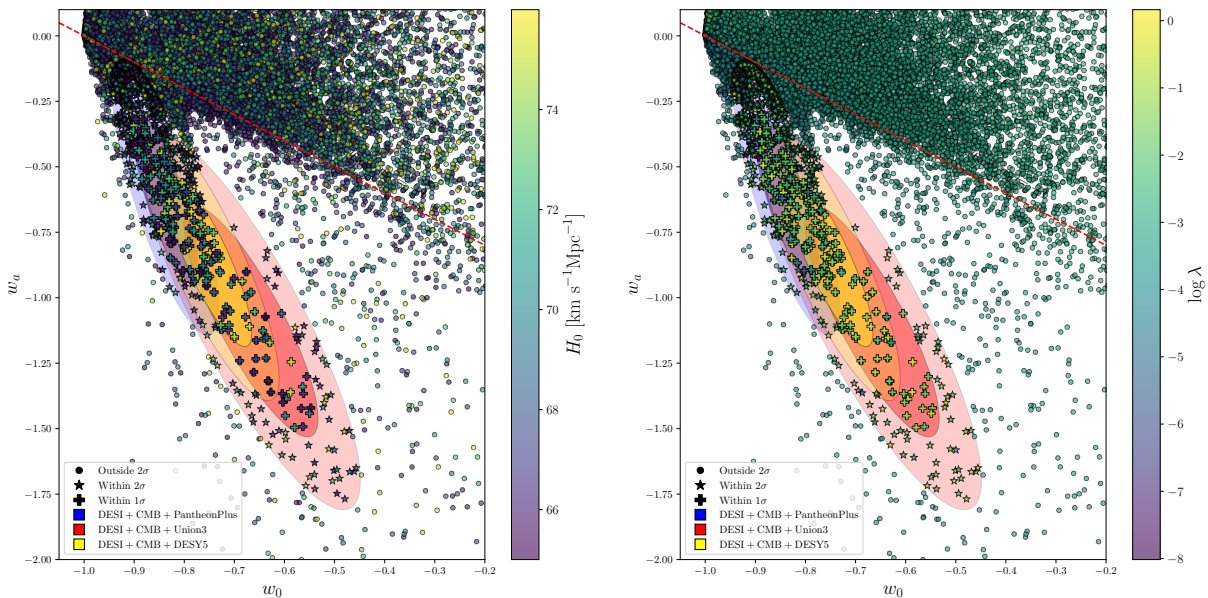


**Figure 5:** Scatter plots in the  $w_0$ - $w_a$  plane overlaid on top of the posterior contours from DESI DR2. The left panel exhibits the Hubble parameter  $H_0$  as the color axis while the right panel shows  $\log \lambda$ . The model is able to produce benchmarks that lie in the  $1\sigma$  and  $2\sigma$  posteriors of the considered data sets.

The left panel of Fig. 5 shows the Hubble parameter  $H_0$  as the color axis while the right panel shows  $\log \lambda$ . The DESI posterior distributions from fits to  $w_0 w_a$ CDM are shown as  $1\sigma$  and  $2\sigma$  ellipses corresponding to three choices of data set combinations. One can see that a large number of model data points are above the  $w_0 + w_a = -1$  line while fewer points are below. Also, a lot of these points fall within the  $1\sigma$  and  $2\sigma$  bounds from DESI. Therefore, quintessence is able to produce values of  $w_0$  and  $w_a$  that are consistent with DESI without having the DE EoS cross the phantom divide. As it was argued in refs. [53, 70, 71], DESI’s results showing an apparent phantom crossing does not mean that there is a violation of the Null Energy Condition (NEC). In fact, this phantom crossing can be a product of extrapolating the CPL parameterization of  $w(a)$  outside the validity region where the distance observations are made and fitted to the model. Note that the authors of ref. [72] have shown that some quintessence models can sometimes lie in the phantom region of the  $w_0$ - $w_a$  plane. The quintessence potentials adopted by the previous references differ from ours, in addition to the fact that our model involves a DM-DE interaction.

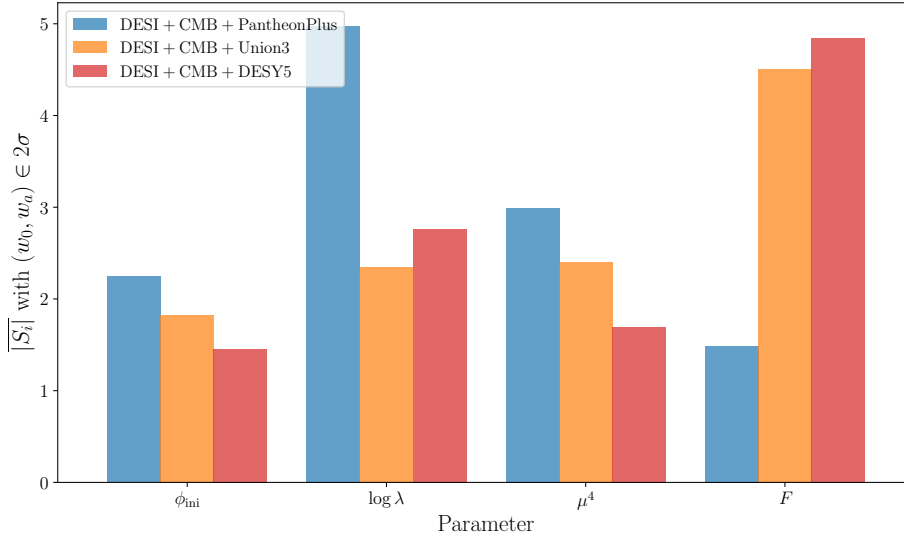


**Figure 6:** The mean absolute Shapley value,  $\overline{|S_i|}$ , of the four model input parameters for the three data sets considered by DESI. The parameter with the largest  $\overline{|S_i|}$  value has the most impact in bringing the  $(w_0, w_a)$  values to within  $2\sigma$  of their experimental value.

Our model contains four input parameters and to determine which parameter has the strongest impact in pushing the  $w_0$  and  $w_a$  values to within  $2\sigma$  of their experimental values determined by DESI, we use SHAP (SHapley Additive exPlanations) [73]. We use the machine learning algorithm XGBoost [74] to train a gradient-boosted decision tree classifier (XGBoostClassifier) on the Monte Carlo data from our model. The algorithm learns how the model input parameters work together to produce points that fall within  $2\sigma$  of DESI’s  $w_0$  and  $w_a$  values. XGBoost builds a model composed of several decision trees equipped with a probability that the classifier has either rendered a point within the experimental limits or not. This information is used by TreeSHAP (part of SHAP), which is a fast algorithm used to compute the exact Shapley values. Each model input parameter is considered a ‘feature’ and the SHAP value can tell us which particular feature in the model has the largest impact on the model prediction or outcome. Let  $f(x)$  be the model prediction for input  $x$ ,  $A$  is the full set of features  $x_i$ ,  $B \subseteq A$  is the set excluding feature  $x_i$  and  $|A|$  ( $|B|$ ) is the number of features in set  $A$  ( $B$ ). The SHAP value for feature  $x_i$  is then

$$S_i(f, x) = \sum_{B \subseteq A \setminus \{i\}} \frac{|B|!(|A| - |B| - 1)!}{|A|!} [f_{B \cup \{i\}}(x) - f_B(x)], \quad (5.14)$$

where  $f_B(x)$  is the model prediction with feature  $x_i$  withheld and  $f_{B \cup \{i\}}(x)$  is the model prediction with the feature included. The mean Shapley values,  $\overline{|S_i|}$ , defined as

$$\overline{|S_i|} = \frac{1}{N} \sum_{j=1}^N |S_i(f, x_j)|, \quad (5.15)$$

where the sum runs over all data points in the sample, is shown in Fig. 6 for the four input parameters:  $\phi_{\text{ini}}$ ,  $\log \lambda$ ,  $\mu^4$  and  $F$ . The analysis is done for DESI’s three data sets that include

PantheonPlus, Union3 and DESY5 and are shown in blue, orange and red, respectively. One can see that for the PantheonPlus data set, the DM-DE interaction strength,  $\lambda$ , has the largest Shapley value which means that this parameter has the largest impact in driving the  $w_0$  and  $w_a$  values to within  $2\sigma$  of their experimental values. For the data sets, Union3 and DESY5, the parameter  $F$  has the largest impact.

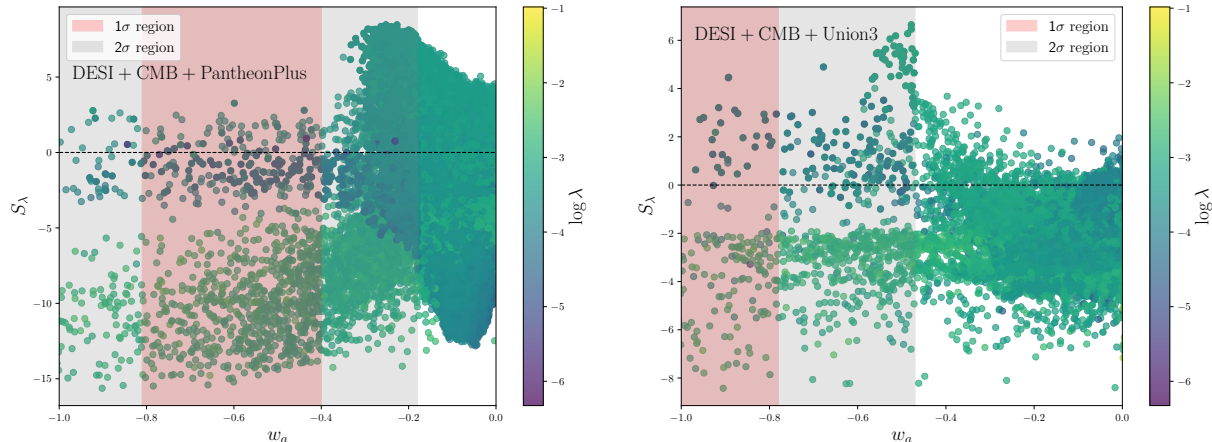


**Figure 7:** A scatter plot of the model data points showing the Shapley value,  $S_\lambda$ , of the DM-DE coupling  $\lambda$  versus the parameter  $w_a$ . The color axis represents the values of  $\log \lambda$ . The analysis in the left panel is done for the DESI+CMB+PantheonPlus data set while the right panel is for the DESI+CMB+Union3 data set.

In the scatter plots of Fig. 7, we show the data points in  $S_\lambda$ - $w_a$  plane (with  $S_\lambda$  the Shapley value of  $\lambda$ ) and the color axis represents the DM-DE interaction strength. The left panel shows the PantheonPlus data set while the right one shows Union3. One can see that for the PantheonPlus data set, the highest density of points for higher  $\lambda$  occurs above  $S_\lambda = 0$  and are concentrated near the upper edge of the  $2\sigma$  region which confirms that  $\lambda$  is an impactful parameter in this data set. However, for the Union3 data set (right panel), most points are below  $S_\lambda = 0$  and the few that have  $S_\lambda > 0$  are characterized by small values of  $\lambda$ .

We give in Table 1 the 68% CL values of the model input parameters and some derived cosmological parameters. The obtained values of  $w_0$ ,  $w_a$ ,  $H_0$  and  $\Omega_m$  agree with DESI's results for each of the three data sets. Compared to the other data sets, the PantheonPlus data set gives the largest upper limit on  $\lambda$  value. We show in the last row the difference in the Deviance Information Criterion (DIC) [75, 76] defined as

$$\Delta(\text{DIC}) = \text{DIC}_{\lambda=0} - \text{DIC}_{\lambda \neq 0} \quad (5.16)$$

One can see that for all three data sets,  $\Delta(\text{DIC}) < 0$  which means that the no interaction model is strongly preferred over the DM-DE interaction scenario.

Parameter	DESI+CMB+PantheonPlus	DESI+CMB+Union3	DESI+CMB+DESY5
$F [m_{\text{Pl}}]$	$1.14^{+1.28}_{-0.57}$	$1.22^{+1.24}_{-0.96}$	$0.336^{+1.082}_{-0.243}$
$\phi_{\text{ini}} [m_{\text{Pl}}]$	$1.11^{+0.22}_{-0.19}$	$1.10^{+0.66}_{-2.22}$	$1.97^{+0.50}_{-1.34}$
$10^8 \mu^4$	$2.86^{+0.61}_{-0.65}$	$2.38^{+1.29}_{-0.39}$	$2.95^{+1.87}_{-1.30}$
$\log \lambda$	$< -2.78$	$< -2.99$	$< -3.26$
$w_0$	$-0.80^{+0.73}_{-0.03}$	$-0.518^{+0.180}_{-0.321}$	$-0.813^{+0.353}_{-0.031}$
$w_a$	$-0.227^{+0.044}_{-0.467}$	$-0.505^{+0.282}_{-0.388}$	$-0.556 \pm 0.366$
$H_0$	$67.97^{+5.83}_{-2.80}$	$68.17^{+5.63}_{-3.10}$	$70.59^{+3.25}_{-4.74}$
$\Omega_m$	$0.308^{+0.027}_{-0.047}$	$0.306^{+0.030}_{-0.045}$	$0.286^{+0.043}_{-0.025}$
$\Delta(\text{DIC})$	-109	-29.6	-71.5

**Table 1:** Constraints on some of the cosmological parameters of our model. The values are quoted at 68% CL intervals, unless an upper or lower bounds are shown, in which case it is the 95% CL interval.

With the DESI DR2 results, we are able to set an upper limit on the DM-DE interaction strength. We show in Fig. 8 the model points that respect the imposed upper limit on  $\lambda$ , as well as constraints on  $H_0$  and  $\Omega_m$ . Many points still populate the  $1\sigma$  and  $2\sigma$  posterior distributions in the  $w_0$ - $w_a$  plane even for  $\lambda$  values close to the upper limit.

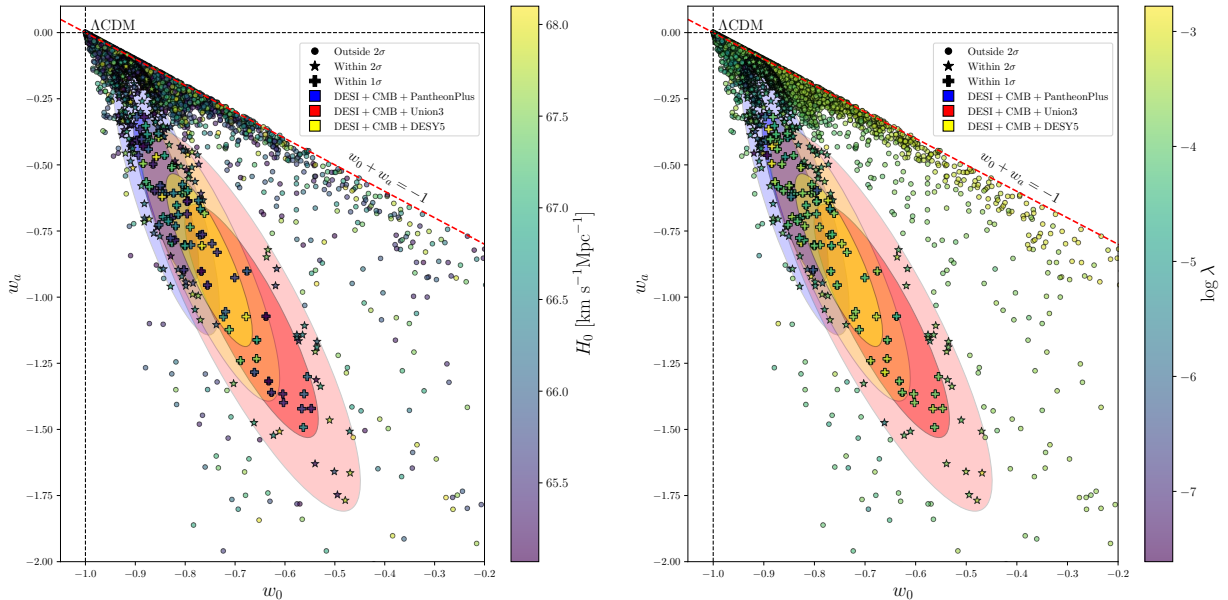


**Figure 8:** Scatter plots in the  $w_0$ - $w_a$  plane similar to Fig. 5 but now with the upper limit on  $\log \lambda$  imposed. To enforce matter domination at the right epoch, only points below  $w_0 + w_a = -1$  are considered. Many of the remaining points still fall within the  $1\sigma$  and  $2\sigma$  experimental constraints.

A final word regarding the calculation of  $\Delta(\text{DIC})$  is warranted. The DIC is determined as  $-2\langle\log \mathcal{L}\rangle + p_D$ , where the first term is the mean deviance and the second term is a penalty on model complexity. Our interacting model has an extra parameter  $\lambda$  over the non-interacting model which gets penalized leading to  $\Delta(\text{DIC}) < 0$ . A future direction for this work would be to investigate field-theoretic interaction terms than can overcome this difficulty, making a DM-DE interaction model more favorable.

## 6 Conclusion

In this work we discussed a field-theoretic model of cosmology with an interaction term between dark matter and dark energy which are described by ultralight spin zero fields. We show that the fluid formalism used to describe dark matter-dark energy interaction is inconsistent in a field-theory approach. Furthermore, considering a specific dark energy potential and a dark matter-dark energy interaction term, we study the cosmological implication of such a model on the evolution of the dark energy equation of state. We distinguish between two regimes based on the DM-DE interaction strength: the strong coupling regime with  $\lambda \geq 10^{-2}$  and the weak coupling region with  $\lambda < 10^{-2}$ . The strong coupling regime induces a transmutation of the dark energy equation of state which is visible in its evolution from a thawing behavior to a scaling freezing behavior. A dark energy equation of state from a freezing quintessence at current times is at odds with the DESI results and so the strong coupling regime can be ruled out. The weak coupling regime, on the other hand, is shown to produce results consistent with DESI, aligned with the prediction of an evolving equation of state. We provide a fit to the dark energy equation of state, which, to leading order in  $(1 - a)$ , can produce  $w_0$  and  $w_a$  values consistent with DESI without crossing the phantom divide. Using the three-data set combinations from DESI, we derive an upper limit on the value of  $\lambda$  and show that many benchmark points close to this upper limit remain consistent with DESI.

**Acknowledgments:** A communication with Kyle S. Dawson is acknowledged. The research of PN was supported in part by the NSF Grant PHY-2209903. The analysis presented here was done using the computing resources of the Phage Cluster at Union College.

## Appendices

Here we give further details of the analysis presented in this work where we discuss the background equations used and further numerical analysis. Thus, we present all the Klein-Gordon equations as well as the dark matter background equations rewritten in terms of angular variables that are used to evolve the background cosmology of the QCDM model. We also give the background equations of the phenomenological model resulting from the  $\sum_i Q_i = 0$  assumption for the sake of comparison with QCDM.

## A Background equations for a general dark matter potential

We give the background evolution equations of dark matter and dark energy for the case of a general dark matter potential. For the interacting quintessence-dark matter model (QCDM),  $\chi$  is a dark matter field while  $\phi$  is a dark energy field. Instead of the DM potential of Eq. (4.1), we consider the general form

$$V_1(\chi) = m_\chi^2 f^2 \left[ 1 + \cos\left(\frac{\chi}{f}\right) \right], \quad (\text{A.1})$$

while that potentials  $V_2(\phi)$  and  $V_{12}(\phi, \chi)$  have the forms of Eqs. (4.2) and (4.3). Define the DM energy density so that  $\tilde{\rho}_\chi = \rho_\chi - V_{12}$  with the modified energy density fraction being  $\tilde{\Omega}_\chi \equiv \tilde{\rho}_\chi/\rho_{\text{cr}}$ . We recast the KG equation for  $\chi$  and  $\phi$ , Eqs. (4.4) and (4.5), in terms of the new variables defined by Eqs. (4.7)–(4.9). We then obtain the differential equations of  $\Omega_\chi = \rho_\chi/\rho_{\text{cr}}$ ,  $\theta$  and  $y$ . For  $\Omega_\chi$  we have

$$\Omega'_\chi = 3\mathcal{H}\Omega_\chi(w_T - w_\chi) + \frac{\kappa^2 a^2}{3\mathcal{H}^2} \left[ \mathcal{H}(1 + 3w_\chi)V_{12} - \chi'V_{12,\chi} \right], \quad (\text{A.2})$$

with the DM equation of state  $w_\chi = -\cos\theta$  and  $w_T = \sum p_i/\sum \rho_i$ , where the sum is over all species (baryons, photons, neutrinos, DM and DE). As for the variables  $\theta$  and  $y$ , we get

$$\theta' = -3\mathcal{H}\sin\theta + \mathcal{H}y - \frac{\kappa^2 a^2}{3\mathcal{H}^2 \tilde{\Omega}_\chi} \left( 2\mathcal{H}V_{12} + \chi'V_{12,\chi} \right) \cot\frac{\theta}{2}, \quad (\text{A.3})$$

and

$$y' = \frac{3}{2}\mathcal{H}(1 + w_T)y + \frac{\beta_\chi}{2}\mathcal{H}\tilde{\Omega}_\chi \sin\theta, \quad (\text{A.4})$$

where  $\beta_\chi \equiv 3/(\kappa^2 f^2)$  and  $\tilde{\Omega}_\chi = \Omega_\chi - (\kappa^2 a^2/3\mathcal{H}^2)V_{12}$ . Note that the last set of terms in each of Eqs. (A.2) and (A.3) represent the interaction term.

Next, we consider the assumption  $Q_\chi = -Q_\phi$  and discuss its impact on cosmology from a field theory perspective. This assumption directly leads to  $V'_{12} = 0$  so that

$$V_{12,\phi}\phi'_0 + V_{12,\chi}\chi'_0 = 0, \quad (\text{A.5})$$

Differentiating Eq. (A.5) with respect to time and using Eq. (4.5) we get

$$V_{12,\chi\chi}\chi_0'^2 + V_{12,\chi}\chi_0'' + V_{12,\phi\phi} \left( \frac{V_{12,\chi}}{V_{12,\phi}} \right)^2 \chi_0'^2 - 2\mathcal{H}V_{12,\phi} \left( -\frac{V_{12,\chi}}{V_{12,\phi}} \chi_0' \right) - a^2 V_{12,\phi} V_{t,\phi} = 0, \quad (\text{A.6})$$

where  $V_t = V_2 + V_{12}$ . Now let us take Eq. (A.5) and differentiate one time with respect to  $\chi$

$$V_{12,\chi\chi}\chi'_0 + V_{12,\chi\phi}\phi'_0 = 0, \quad (\text{A.7})$$

and then another with respect to  $\phi$

$$V_{12,\phi\chi}\chi'_0 + V_{12,\phi\phi}\phi'_0 = 0. \quad (\text{A.8})$$

Eliminating  $V_{12,\phi\chi}$  from both equations gives

$$V_{12,\chi\chi} = V_{12,\phi\phi} \left( \frac{V_{12,\chi}}{V_{12,\phi}} \right)^2. \quad (\text{A.9})$$

Using this result in Eq. (A.6), we get

$$\chi''_0 + 2\mathcal{H}\chi'_0 + \frac{2V_{12,\chi\chi}}{V_{12,\chi}}\chi_0'^2 - a^2 \frac{V_{12,\phi}V_{t,\phi}}{V_{12,\chi}} = 0, \quad (\text{A.10})$$

which is a different equation from the KG equation of  $\chi$ , i.e., Eq. (4.4). However, the field  $\chi$  cannot obey two different KG equations. Setting Eq. (A.10) equal to Eq. (4.4) gives

$$\chi_0'^2 = \frac{a^2 V_{12,\chi}}{2V_{12,\chi\chi}} \left( V_{1,\chi} + V_{12,\chi} + \frac{V_{12,\phi}V_{t,\phi}}{V_{12,\chi}} \right). \quad (\text{A.11})$$

Since  $V_{12} = \frac{\lambda}{2}\chi^2\phi^2 = \text{constant}$  implies that  $\chi^2\phi^2 = c$ , where  $c$  is a constant of time. In this case, Eq. (A.11) becomes

$$\chi_0'^2 = \frac{a^2}{2}\chi_0 \left( V_{1,\chi} + V_{12,\chi} + \frac{\chi_0}{\phi_0} V_{t,\phi} \right). \quad (\text{A.12})$$

Using Eq. (4.6), Eq. (A.12) and Eqs. (4.7)–(4.9), we get a new set of differential equations

$$\begin{aligned} \Omega'_\chi &= 3\mathcal{H}\tilde{\Omega}_\chi(1 + w_T) - \frac{5}{8}\mathcal{H}\tilde{\Omega}_\chi y \sin\theta + \frac{\kappa^2 a^2}{2\mathcal{H}}\lambda c(1 + w_T) \\ &+ \frac{\sqrt{6}\kappa a^2}{12\mathcal{H}}\tilde{\Omega}_\chi^{1/2}\mathcal{V}_1 \sin\frac{\theta}{2} - \frac{\kappa^2 a^2}{12\mathcal{H}^2}c\frac{\phi'_0}{\phi_0^3}\mathcal{V}_2 - \frac{\kappa^2}{48}cY, \end{aligned} \quad (\text{A.13})$$

and

$$\theta' = \frac{1}{8}\mathcal{H}y(3 - 5\cos\theta) + \frac{\sqrt{6}\kappa a^2}{12\mathcal{H}\tilde{\Omega}_\chi^{1/2}}\mathcal{V}_1 \cos\frac{\theta}{2} - \frac{\kappa^2 a^2}{12\mathcal{H}^2\tilde{\Omega}_\chi}c\frac{\phi'_0}{\phi_0^3}\mathcal{V}_2 \cot\frac{\theta}{2} - \frac{\kappa^2}{48\tilde{\Omega}_\chi}cY \cot\frac{\theta}{2}, \quad (\text{A.14})$$

where

$$\mathcal{V}_1 = \frac{2V_{2,\phi}}{\phi_0} + \frac{2\lambda c}{\phi_0^2} - V_{2,\phi\phi}, \quad (\text{A.15})$$

$$\mathcal{V}_2 = \lambda\phi_0^2 + \frac{V_{2,\phi}}{\phi_0} + \frac{\lambda c}{\phi_0^2}, \quad (\text{A.16})$$

$$Y = \frac{\phi'_0}{\phi_0^3} \left[ y^2 - \beta_\chi \tilde{\Omega}_\chi(1 + \cos\theta) \right]. \quad (\text{A.17})$$

Here one finds that the new Eqs. (A.13) and (A.14) are driven by the DE potential and the solution to the KG equation of  $\phi$ . Due to the constraint  $V_{12} = \lambda c/2$ , one can determine an equation for  $y$  so that

$$y = \frac{4}{\mathcal{H}}\frac{\phi'_0}{\phi_0} \tan\frac{\theta}{2} - \frac{2\kappa^2 a^2}{3\mathcal{H}^3\tilde{\Omega}_\chi \sin\theta}c\frac{\phi'_0}{\phi_0^3}\mathcal{V}_2. \quad (\text{A.18})$$

## B Comparison between QCDM and the phenomenological model

The phenomenological model based fluid equations assume that  $Q_\chi = -Q_\phi$  which, as was shown in this work, is in contradiction with the field theory approach. To compare the results from this phenomenological model with that of QCDM, we show in Fig. 9 the same plots of energy density and equations of state as in Fig. 1. The obtained trend is similar to that of normal cosmology but here one can see an important difference relative to the QCDM analysis concerning matter-radiation equality which is attained at  $z_{\text{eq}} \sim 532$ , in disagreement with Planck's result. Another important difference can also be seen from the evolution of the DM equation of state in the lower left panel of Fig. 9 (dashed line). One can clearly see that the EoS takes a value of  $-1$  throughout the evolution and so the DM field acts as DE. This is the main reason for getting an inconsistent cosmology resulting in a very late matter-radiation equality.

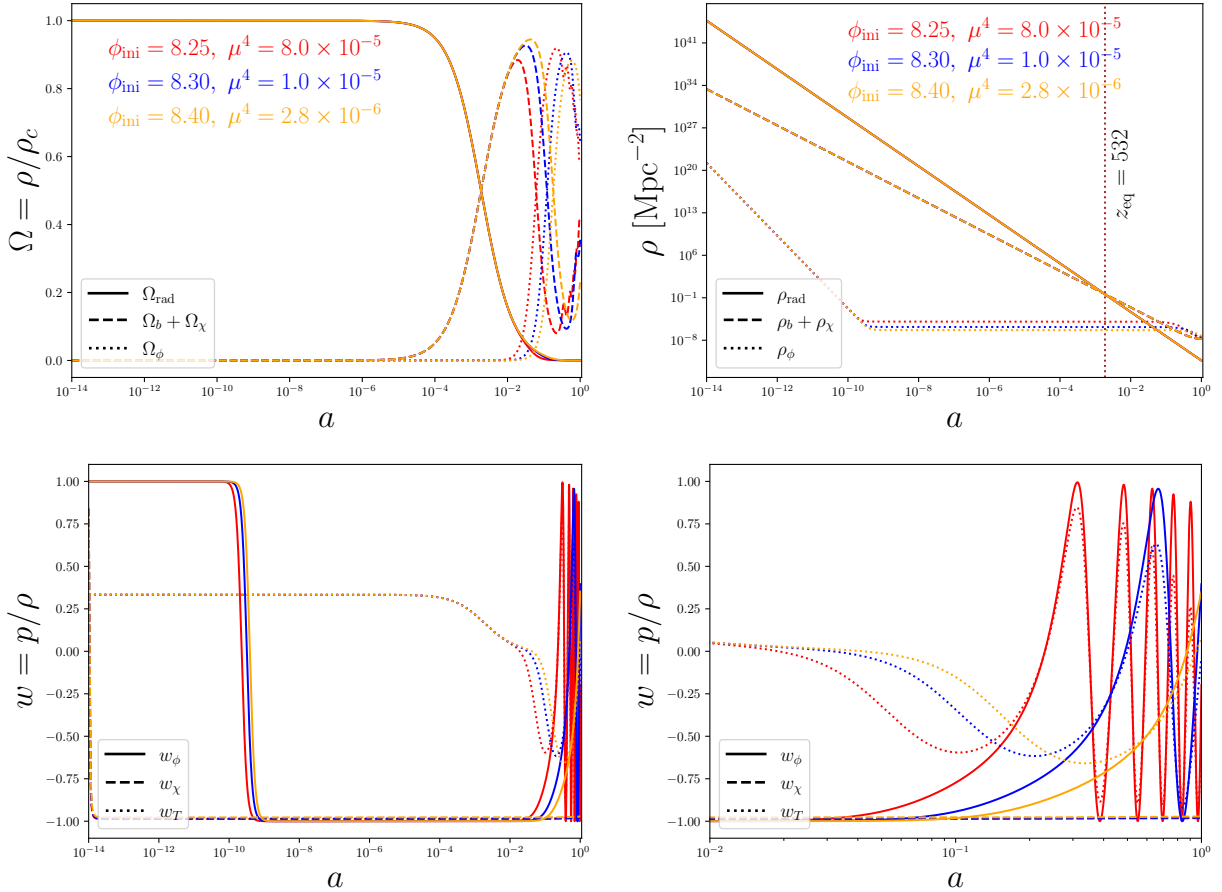


**Figure 9:** Results from the second scenario. Plots of the energy density fraction (top left) and the energy density (top right) of all species and the equations of state (EoS) of DM and DE and the total EoS (bottom panels) as a function of the scale factor  $a$ . The color code in the top panels is the same for all panels and correspond to different values of  $\phi_{\text{ini}}$  and  $\mu^4$ , expressed in standard CLASS units of  $m_{\text{pl}}$  and  $m_{\text{pl}}^2/\text{Mpc}^2$ , respectively.

## C Correlation plots

In Figs. 10 and 11, we show the correlation plots between the different parameters of the model. From Fig. 10, one can see a strong positive correlation between  $\lambda$  and  $w_0$  but a weaker negative correlation between  $\lambda$  and  $w_a$ . However, the latter has a stronger positive correlation with  $\mu^4$ . So one sees that the interplay between different parameters of the model can bring concordance with DESI DR2. A larger set of parameters is shown in Fig. 11. One important observation that can be made is that  $H_0$  and  $w_0$  are not anti-correlated as is usually seen in uncoupled quintessence models [29, 77] as well as in some coupled quintessence [78]. A field-theoretic interaction term results in a very mild positive correlation between  $H_0$  and  $w_0$ . This is, however, still not sufficient to explain the Hubble tension.

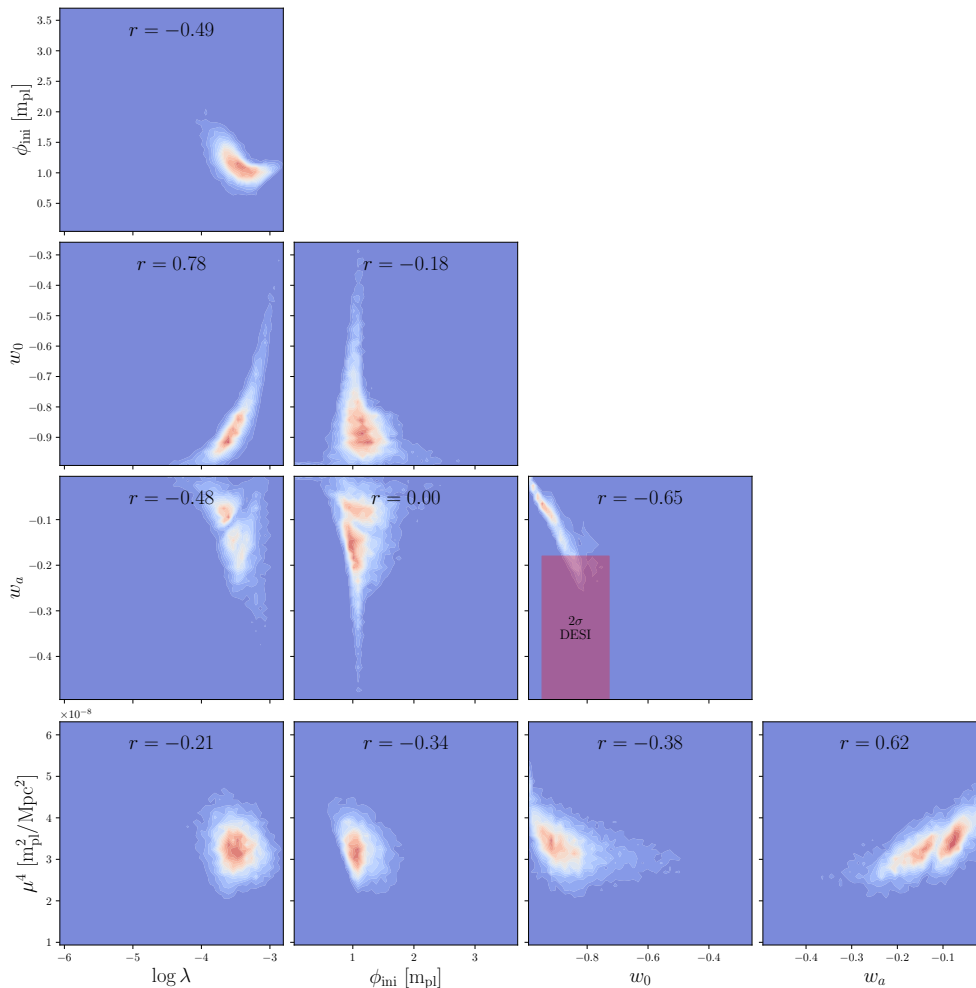


**Figure 10:** Triangle plots showing the correlations between different input and output parameters of the model. Notice the strong positive correlation between  $\lambda$  and  $w_0$  and between  $\mu^4$  and  $w_a$ . A mild negative correlation exists between  $\lambda$  and  $w_a$ .

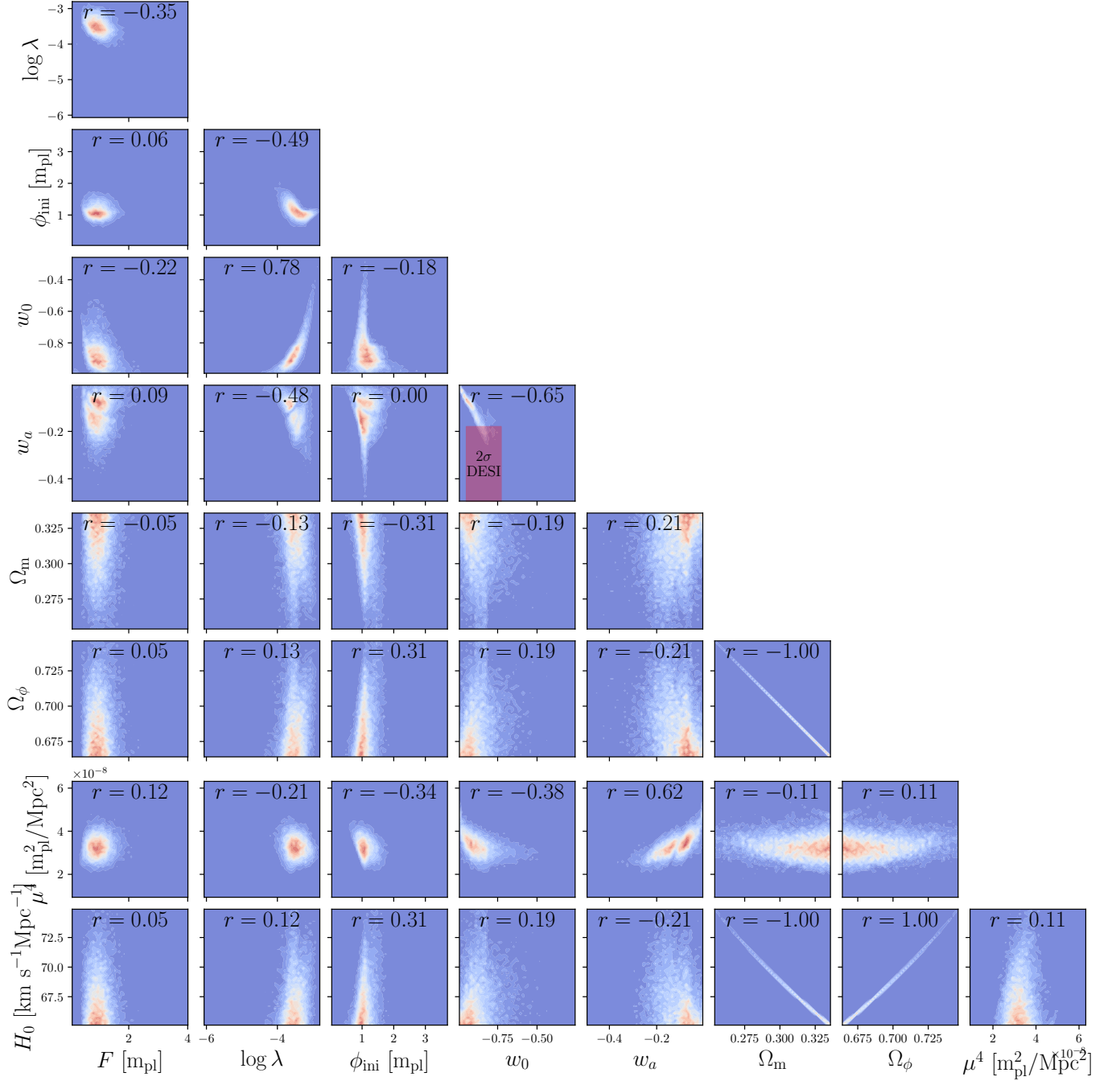


**Figure 11:** Same as in Fig. 10 but now considering a larger set of input and output parameters.

## References

- [1] E. Abdalla, G. Franco Abellán, A. Aboubrahim, A. Agnello, O. Akarsu, Y. Akrami, G. Alestas, D. Aloni, L. Amendola and L. A. Anchordoqui, *et al.* JHEAp **34**, 49-211 (2022) doi:10.1016/j.jheap.2022.04.002 [arXiv:2203.06142 [astro-ph.CO]].

- [2] E. Di Valentino, J. Levi Said, A. Riess, A. Pollo, V. Poulin, A. Gómez-Valent, A. Weltman, A. Palmese, C. D. Huang and C. van de Bruck, *et al.* [arXiv:2504.01669 [astro-ph.CO]].
- [3] A. Pourtsidou, C. Skordis and E. J. Copeland, Phys. Rev. D **88**, no.8, 083505 (2013) doi:10.1103/PhysRevD.88.083505 [arXiv:1307.0458 [astro-ph.CO]].
- [4] A. Pourtsidou and T. Tram, Phys. Rev. D **94**, no.4, 043518 (2016) doi:10.1103/PhysRevD.94.043518 [arXiv:1604.04222 [astro-ph.CO]].
- [5] M. S. Linton, A. Pourtsidou, R. Crittenden and R. Maartens, JCAP **04**, 043 (2018) doi:10.1088/1475-7516/2018/04/043 [arXiv:1711.05196 [astro-ph.CO]].
- [6] F. N. Chamings, A. Avgoustidis, E. J. Copeland, A. M. Green and A. Pourtsidou, Phys. Rev. D **101**, no.4, 043531 (2020) doi:10.1103/PhysRevD.101.043531 [arXiv:1912.09858 [astro-ph.CO]].
- [7] S. Pan, W. Yang, E. Di Valentino, E. N. Saridakis and S. Chakraborty, Phys. Rev. D **100**, no.10, 103520 (2019) doi:10.1103/PhysRevD.100.103520 [arXiv:1907.07540 [astro-ph.CO]].
- [8] M. Bonici and N. Maggiore, Eur. Phys. J. C **79**, no.8, 672 (2019) doi:10.1140/epjc/s10052-019-7198-1 [arXiv:1812.11176 [gr-qc]].
- [9] W. Yang, O. Mena, S. Pan and E. Di Valentino, Phys. Rev. D **100**, no.8, 083509 (2019) doi:10.1103/PhysRevD.100.083509 [arXiv:1906.11697 [astro-ph.CO]].
- [10] S. Pan, G. S. Sharov and W. Yang, Phys. Rev. D **101**, no.10, 103533 (2020) doi:10.1103/PhysRevD.101.103533 [arXiv:2001.03120 [astro-ph.CO]].
- [11] B. Wang, E. Abdalla, F. Atrio-Barandela and D. Pavon, Rept. Prog. Phys. **79**, no.9, 096901 (2016) doi:10.1088/0034-4885/79/9/096901 [arXiv:1603.08299 [astro-ph.CO]].
- [12] B. Wang, E. Abdalla, F. Atrio-Barandela and D. Pavón, Rept. Prog. Phys. **87**, no.3, 036901 (2024) doi:10.1088/1361-6633/ad2527 [arXiv:2402.00819 [astro-ph.CO]].
- [13] C. G. Boehmer, N. Tamanini and M. Wright, Phys. Rev. D **91**, no.12, 123002 (2015) doi:10.1103/PhysRevD.91.123002 [arXiv:1501.06540 [gr-qc]].
- [14] C. G. Boehmer, N. Tamanini and M. Wright, Phys. Rev. D **91**, no.12, 123003 (2015) doi:10.1103/PhysRevD.91.123003 [arXiv:1502.04030 [gr-qc]].
- [15] W. J. Potter and S. Chongchitnan, JCAP **09**, 005 (2011) doi:10.1088/1475-7516/2011/09/005 [arXiv:1108.4414 [astro-ph.CO]].
- [16] E. Di Valentino, A. Melchiorri, O. Mena and S. Vagnozzi, Phys. Rev. D **101**, no.6, 063502 (2020) doi:10.1103/PhysRevD.101.063502 [arXiv:1910.09853 [astro-ph.CO]].
- [17] E. Di Valentino, A. Melchiorri, O. Mena and S. Vagnozzi, Phys. Dark Univ. **30**, 100666 (2020) doi:10.1016/j.dark.2020.100666 [arXiv:1908.04281 [astro-ph.CO]].

- [18] L. A. Escamilla, O. Akarsu, E. Di Valentino and J. A. Vazquez, JCAP **11**, 051 (2023) doi:10.1088/1475-7516/2023/11/051 [arXiv:2305.16290 [astro-ph.CO]].
- [19] A. Bernui, E. Di Valentino, W. Giarè, S. Kumar and R. C. Nunes, Phys. Rev. D **107**, no.10, 103531 (2023) doi:10.1103/PhysRevD.107.103531 [arXiv:2301.06097 [astro-ph.CO]].
- [20] W. Yang, S. Pan, O. Mena and E. Di Valentino, JHEAp **40**, 19-40 (2023) doi:10.1016/j.jheap.2023.09.001 [arXiv:2209.14816 [astro-ph.CO]].
- [21] L. Amendola, Phys. Rev. D **62**, 043511 (2000) doi:10.1103/PhysRevD.62.043511 [arXiv:astro-ph/9908023 [astro-ph]].
- [22] R. Kase and S. Tsujikawa, Phys. Rev. D **101**, no.6, 063511 (2020) doi:10.1103/PhysRevD.101.063511 [arXiv:1910.02699 [gr-qc]].
- [23] P. Pérez, U. Nucamendi and R. De Arcia, Eur. Phys. J. C **81**, no.12, 1063 (2021) doi:10.1140/epjc/s10052-021-09857-4 [arXiv:2104.07690 [gr-qc]].
- [24] G. Garcia-Arroyo, L. A. Ureña-López and J. A. Vázquez, Phys. Rev. D **110**, no.2, 023529 (2024) doi:10.1103/PhysRevD.110.023529 [arXiv:2402.08815 [astro-ph.CO]].
- [25] J. Beyer, S. Nurmi and C. Wetterich, Phys. Rev. D **84**, 023010 (2011) doi:10.1103/PhysRevD.84.023010 [arXiv:1012.1175 [astro-ph.CO]].
- [26] J. Beyer, [arXiv:1407.0497 [astro-ph.CO]].
- [27] C. van de Bruck, G. Poulot and E. M. Teixeira, JCAP **07**, 019 (2023) doi:10.1088/1475-7516/2023/07/019 [arXiv:2211.13653 [hep-th]].
- [28] W. Yang, S. Pan, E. Di Valentino, R. C. Nunes, S. Vagnozzi and D. F. Mota, JCAP **09**, 019 (2018) doi:10.1088/1475-7516/2018/09/019 [arXiv:1805.08252 [astro-ph.CO]].
- [29] B. H. Lee, W. Lee, E. Ó. Colgáin, M. M. Sheikh-Jabbari and S. Thakur, JCAP **04**, no.04, 004 (2022) doi:10.1088/1475-7516/2022/04/004 [arXiv:2202.03906 [astro-ph.CO]].
- [30] M. Doran and G. Robbers, JCAP **06**, 026 (2006) doi:10.1088/1475-7516/2006/06/026 [arXiv:astro-ph/0601544 [astro-ph]].
- [31] P. Agrawal, F. Y. Cyr-Racine, D. Pinner and L. Randall, Phys. Dark Univ. **42**, 101347 (2023) doi:10.1016/j.dark.2023.101347 [arXiv:1904.01016 [astro-ph.CO]].
- [32] S. Vagnozzi, Universe **9**, no.9, 393 (2023) doi:10.3390/universe9090393 [arXiv:2308.16628 [astro-ph.CO]].
- [33] Z. Berezhiani, A. D. Dolgov and I. I. Tkachev, Phys. Rev. D **92**, no.6, 061303 (2015) doi:10.1103/PhysRevD.92.061303 [arXiv:1505.03644 [astro-ph.CO]].
- [34] A. Ibarra, D. Tran and C. Weniger, Int. J. Mod. Phys. A **28**, 1330040 (2013) doi:10.1142/S0217751X13300408 [arXiv:1307.6434 [hep-ph]].
- [35] A. Aboubrahim, M. Klasen and P. Nath, JCAP **04**, no.04, 042 (2022) doi:10.1088/1475-7516/2022/04/042 [arXiv:2202.04453 [astro-ph.CO]].

- [36] E. Fernandez-Martinez, M. Pierre, E. Pinsard and S. Rosauero-Alcaraz, *Eur. Phys. J. C* **81**, no.10, 954 (2021) doi:10.1140/epjc/s10052-021-09760-y [arXiv:2106.05298 [hep-ph]].
- [37] M. Escudero and S. J. Witte, *Eur. Phys. J. C* **81**, no.6, 515 (2021) doi:10.1140/epjc/s10052-021-09276-5 [arXiv:2103.03249 [hep-ph]].
- [38] D. Baumann, D. Green, J. Meyers and B. Wallisch, *JCAP* **01**, 007 (2016) doi:10.1088/1475-7516/2016/01/007 [arXiv:1508.06342 [astro-ph.CO]].
- [39] C. Brust, Y. Cui and K. Sigurdson, *JCAP* **08**, 020 (2017) doi:10.1088/1475-7516/2017/08/020 [arXiv:1703.10732 [astro-ph.CO]].
- [40] N. Blinov and G. Marques-Tavares, *JCAP* **09**, 029 (2020) doi:10.1088/1475-7516/2020/09/029 [arXiv:2003.08387 [astro-ph.CO]].
- [41] T. D. Jacques, L. M. Krauss and C. Lunardini, *Phys. Rev. D* **87**, no.8, 083515 (2013) [erratum: *Phys. Rev. D* **88**, no.10, 109901 (2013)] doi:10.1103/PhysRevD.87.083515 [arXiv:1301.3119 [astro-ph.CO]].
- [42] A. J. Cuesta, M. E. Gómez, J. I. Illana and M. Masip, *JCAP* **04**, no.04, 009 (2022) doi:10.1088/1475-7516/2022/04/009 [arXiv:2109.07336 [hep-ph]].
- [43] S. Vagnozzi, *Phys. Rev. D* **102**, no.2, 023518 (2020) doi:10.1103/PhysRevD.102.023518 [arXiv:1907.07569 [astro-ph.CO]].
- [44] J. Valiviita, E. Majerotto and R. Maartens, *JCAP* **07**, 020 (2008) doi:10.1088/1475-7516/2008/07/020 [arXiv:0804.0232 [astro-ph]].
- [45] M. B. Gavela, D. Hernandez, L. Lopez Honorez, O. Mena and S. Rigolin, *JCAP* **07**, 034 (2009) [erratum: *JCAP* **05**, E01 (2010)] doi:10.1088/1475-7516/2009/07/034 [arXiv:0901.1611 [astro-ph.CO]].
- [46] A. G. Adame *et al.* [DESI], *JCAP* **02**, 021 (2025) doi:10.1088/1475-7516/2025/02/021 [arXiv:2404.03002 [astro-ph.CO]].
- [47] M. Abdul Karim *et al.* [DESI], [arXiv:2503.14738 [astro-ph.CO]].
- [48] M. Chevallier and D. Polarski, *Int. J. Mod. Phys. D* **10**, 213-224 (2001) doi:10.1142/S0218271801000822 [arXiv:gr-qc/0009008 [gr-qc]].
- [49] E. V. Linder, *Phys. Rev. Lett.* **90**, 091301 (2003) doi:10.1103/PhysRevLett.90.091301 [arXiv:astro-ph/0208512 [astro-ph]].
- [50] R. J. Scherrer and A. A. Sen, *Phys. Rev. D* **77**, 083515 (2008) doi:10.1103/PhysRevD.77.083515 [arXiv:0712.3450 [astro-ph]].
- [51] R. R. Caldwell and E. V. Linder, *Phys. Rev. Lett.* **95**, 141301 (2005) doi:10.1103/PhysRevLett.95.141301 [arXiv:astro-ph/0505494 [astro-ph]].
- [52] W. J. Wolf and P. G. Ferreira, *Phys. Rev. D* **108**, no.10, 103519 (2023) doi:10.1103/PhysRevD.108.103519 [arXiv:2310.07482 [astro-ph.CO]].

- [53] W. J. Wolf, C. García-García, D. J. Bartlett and P. G. Ferreira, *Phys. Rev. D* **110**, no.8, 083528 (2024) doi:10.1103/PhysRevD.110.083528 [arXiv:2408.17318 [astro-ph.CO]].
- [54] P. G. Ferreira and M. Joyce, *Phys. Rev. D* **58**, 023503 (1998) doi:10.1103/PhysRevD.58.023503 [arXiv:astro-ph/9711102 [astro-ph]].
- [55] E. J. Copeland, A. R. Liddle and D. Wands, *Phys. Rev. D* **57**, 4686-4690 (1998) doi:10.1103/PhysRevD.57.4686 [arXiv:gr-qc/9711068 [gr-qc]].
- [56] A. Aboubrahim and P. Nath, *JCAP* **09**, 076 (2024) doi:10.1088/1475-7516/2024/09/076 [arXiv:2406.19284 [astro-ph.CO]].
- [57] A. Aboubrahim and P. Nath, [arXiv:2503.09769 [astro-ph.CO]].
- [58] G. Pantazis, S. Nesseris and L. Perivolaropoulos, *Phys. Rev. D* **93**, no.10, 103503 (2016) doi:10.1103/PhysRevD.93.103503 [arXiv:1603.02164 [astro-ph.CO]].
- [59] S. Tsujikawa, *Class. Quant. Grav.* **30**, 214003 (2013) doi:10.1088/0264-9381/30/21/214003 [arXiv:1304.1961 [gr-qc]].
- [60] M. S. Turner, *Phys. Rev. D* **28**, 1243 (1983) doi:10.1103/PhysRevD.28.1243
- [61] L. A. Ureña-López and A. X. Gonzalez-Morales, *JCAP* **07**, 048 (2016) doi:10.1088/1475-7516/2016/07/048 [arXiv:1511.08195 [astro-ph.CO]].
- [62] D. Blas, J. Lesgourgues and T. Tram, *JCAP* **07**, 034 (2011) doi:10.1088/1475-7516/2011/07/034 [arXiv:1104.2933 [astro-ph.CO]].
- [63] J. A. Frieman, C. T. Hill, A. Stebbins and I. Waga, *Phys. Rev. Lett.* **75**, 2077-2080 (1995) doi:10.1103/PhysRevLett.75.2077 [arXiv:astro-ph/9505060 [astro-ph]].
- [64] Y. Tada and T. Terada, *Phys. Rev. D* **109**, no.12, L121305 (2024) doi:10.1103/PhysRevD.109.L121305 [arXiv:2404.05722 [astro-ph.CO]].
- [65] J. Rebouças, D. H. F. de Souza, K. Zhong, V. Miranda and R. Rosenfeld, *JCAP* **02**, 024 (2025) doi:10.1088/1475-7516/2025/02/024 [arXiv:2408.14628 [astro-ph.CO]].
- [66] K. V. Berghaus, J. A. Kable and V. Miranda, *Phys. Rev. D* **110**, no.10, 103524 (2024) doi:10.1103/PhysRevD.110.103524 [arXiv:2404.14341 [astro-ph.CO]].
- [67] W. J. Wolf, P. G. Ferreira and C. García-García, *Phys. Rev. D* **111**, no.4, L041303 (2025) doi:10.1103/PhysRevD.111.L041303 [arXiv:2409.17019 [astro-ph.CO]].
- [68] I. D. Gialamas, G. Hütsi, K. Kannike, A. Racioppi, M. Raidal, M. Vasar and H. Veermäe, *Phys. Rev. D* **111**, no.4, 043540 (2025) doi:10.1103/PhysRevD.111.043540 [arXiv:2406.07533 [astro-ph.CO]].
- [69] P. G. Ferreira and M. Joyce, *Phys. Rev. Lett.* **79**, 4740-4743 (1997) doi:10.1103/PhysRevLett.79.4740 [arXiv:astro-ph/9707286 [astro-ph]].
- [70] O. F. Ramadan, J. Sakstein and D. Rubin, *Phys. Rev. D* **110**, no.4, L041303 (2024) doi:10.1103/PhysRevD.110.L041303 [arXiv:2405.18747 [astro-ph.CO]].

- [71] M. Cortês and A. R. Liddle, JCAP **12**, 007 (2024) doi:10.1088/1475-7516/2024/12/007 [arXiv:2404.08056 [astro-ph.CO]].
- [72] D. Shlivko and P. J. Steinhardt, Phys. Lett. B **855**, 138826 (2024) doi:10.1016/j.physletb.2024.138826 [arXiv:2405.03933 [astro-ph.CO]].
- [73] S. Lundberg and S. I. Lee, [arXiv:1705.07874 [cs.AI]].
- [74] T. Chen and C. Guestrin, doi:10.1145/2939672.2939785 [arXiv:1603.02754 [cs.LG]].
- [75] D. J. Spiegelhalter, N. G. Best, B. P. Carlin and A. van der Linde, J. Roy. Statist. Soc. B **64**, no.4, 583-639 (2002) doi:10.1111/1467-9868.00353
- [76] R. Trotta, Contemp. Phys. **49**, 71-104 (2008) doi:10.1080/00107510802066753 [arXiv:0803.4089 [astro-ph]].
- [77] A. Banerjee, H. Cai, L. Heisenberg, E. Ó. Colgáin, M. M. Sheikh-Jabbari and T. Yang, Phys. Rev. D **103**, no.8, L081305 (2021) doi:10.1103/PhysRevD.103.L081305 [arXiv:2006.00244 [astro-ph.CO]].
- [78] S. Das, P. S. Corasaniti and J. Khoury, Phys. Rev. D **73**, 083509 (2006) doi:10.1103/PhysRevD.73.083509 [arXiv:astro-ph/0510628 [astro-ph]].